Hindawi
Advances in Civil Engineering
Volume 2018, Article ID 8681529, 12 pages
https://doi.org/10.1155/2018/8681529

Research Article

Fatigue Characteristics of Limestone under Triaxial Compression with Cyclic Loading

Yongjie Yang, Huiqiang Duan, Luyi Xing, Shan Ning, and Jiakun Lv

College of Mining and Safety Engineering, Shandong University of Science and Technology, Qingdao 266590, China

Correspondence should be addressed to Huiqiang Duan; duanhuiqiang11@163.com

Received 12 April 2018; Accepted 31 July 2018; Published 2 September 2018

Academic Editor: Wei Wu

This paper presents an experimental investigation of the fatigue properties of limestone subjected to triaxial compression with axial cyclic loading. Tests were conducted on intact limestone samples with a loading frequency of 0.5 Hz and a confining pressure of 10 MPa. The test results show the following five points. (1) Under triaxial conditions, the axial and circumferential deformations at the failure point induced by cyclic loading are slightly larger than the corresponding deformations at the peak stress achieved by conventional compression tests. (2) The first level cyclic loading process has a strong influence on rock deformation in the primary phase during subsequent level cyclic loading. A smaller difference in stress amplitude between the two loading stress levels leads to less deformation during the latter. (3) Circumferential and volumetric changes are more sensitive to fatigue failure in terms of deformation and strain rate than axial changes. (4) The three phases of dissipated energy evolution are consistent with a sample's deformation such that the energy dissipation characteristics reflect the fatigue damage evolution process. (5) A new damage formula is proposed that can concisely describe a rock's zero-cycle damage and damage evolution.

1. Introduction

Repeated stress induced by mining and excavation activities has an unfavorable influence on the stability of zones within underground mines, including the district rise entry into the rock mass, shared haulage and connecting roadways in the floor rock mass of the working face, and within rock surrounding the working face. Repeated mining stress leads to a constant increase of rock deformation and damage and a decrease of its long-term strength, which ultimately results in instabilities and rock failure [1]. Mining stress generally increases with depth and mine development such that a rock mass (pillar) is destroyed by the multilevel amplitude cyclic loading. The cycling of mining-induced stress is much longer than that in laboratory tests, and the loading-unloading process is also more complicated and accompanied by other dynamic loads. Laboratory tests are therefore limited in their ability to reproduce the true rock stress environment; however, similar periodic stresses can be simplified as cyclic loading, and the study of the rock fatigue failure process under loading-unloading remains a safe and efficient method. Furthermore, laboratory findings can be used to evaluate the stability of rock mass and prevent mining disasters and accidents.

Previous studies have employed a variety of tests to analyze the fatigue behavior of different rock types. For example, in uniaxial or triaxial cyclic loading test, rock strain can be divided into three phases: initial, steady, and acceleration [2–5]. Liu and He [6] studied the effects of confining pressure on the deformation properties of intact rock. They found that the axial strain at failure increased with confining pressure, as did residual volumetric strain when dilatancy occurred. Some studies reported that lateral deformation is more sensitive than axial deformation in uniaxial or triaxial cyclic loading test [7, 8]. The experimental results of Feng et al. [9] showed that rock fatigue failure is strongly influenced by the peak stress and stress amplitude of cyclic loading and that fatigue life decreases with increasing peak stress or stress amplitude. Shi et al. [10] studied the effects of static deviatory stress and vibration frequency on the fatigue properties of water-rich mudstone. They found that irreversible cumulative deformation increases with static deviatory stress under the same dynamic stress and that lower frequencies result in larger sample deformation when other

variables are kept constant. Bagde and Petroš [11] suggested that some materials become stronger and more ductile under dynamic cyclic loading, while others become weaker and more brittle. Fuenkajorn and Phueakphum [12] conducted a series of static and cyclic loading tests on rock salt and reported that compressive strength decreased with increasing loading cycle number. During the first few cycles, the rock salt elastic modulus decreased slightly and then remained constant until failure. Liang et al. [13] studied the effects of strain rate on rock salt mechanical properties. Their findings demonstrate that the loading strain rate only slightly affects rock strength and that the elastic modulus increases slightly with increasing strain rate, although the increment was small. Jiang et al. [14] studied rock salt fatigue failure under discontinuous cyclic loading and showed that discontinuous fatigue contributes to the development of residual strain. The fatigue life of samples that underwent interval fatigue tests was significantly shorter than that of samples that only experienced conventional fatigue tests. Fan et al. [15] studied the acoustic emissions (AEs) from salt in conventional fatigue tests (CFTs) and discontinuous cyclic loading tests with loading paths containing zero loading stress intervals (ZLIs). In the CFTs, the AE counting rate gradually decreased and reached a plateau before a rapid increase immediately before failure; however, in the ZLI tests, the maximum counting rate progressively increased until the failure-showing cycles. He et al. [16] reported on the energy dissipated by rocks subjected to cyclic loading and found that both axial strain and energy dissipation evolve through three phases when the peak stress of cyclic loading exceeds the fatigue strength of sandstone.

There have also been some notable achievements in the calculation methodology of the fatigue damage variable. For example, Xie et al. [17] proposed the modified elastic modulus method, Li et al. [18] put forward a formula using the axial strain method, while, Xiao et al. [19, 20] suggested an inverted S-shaped nonlinear fatigue cumulative model. Xiao et al. [21] provide a good review of calculation methods for determining the damage variable. However, the above-cited papers mainly analyzed the fatigue properties of rock materials subjected to constant amplitude cyclic loading, and there have been few studies on deformation and damage evolution under multilevel amplitude cyclic loading. In this paper, we investigate the mechanical properties of limestone in multilevel amplitude cyclic loading tests under a single confining pressure. We propose a concise damage calculation formula, which can provide a theoretical basis for evaluating rock stability with a practical and valuable application to engineering.

2. Materials and Methods

2.1. Starting Material. Limestone samples were collected from a coal mine in Shandong, China. The length and diameter of the cylindrical samples were about 100 and 50 mm, respectively. The samples were strictly prepared according to the International Society for Rock Mechanics (ISRM). After preparation, samples without cracks or joints were selected for testing.

2.2. Experimental Procedures. The tests were conducted using an MTS815.02 servo-controlled rock mechanics test system (MTS Systems Corporation, Eden Prairie, MN, USA), as shown in Figure 1. The triaxial compression tests were performed in both a conventional manner and with cyclic loading. The confining pressure was 10 MPa, and the loading rate was 0.05 MPa/s. The conventional triaxial compression tests were carried out in the displacement-control mode with a loading rate of 0.003 mm/s. The aim of these tests was to obtain complete stress-strain curves and determine the strengths of the limestone samples, thereby providing essential data for subsequent cyclic loading tests.

The triaxial compression tests with cyclic loading were performed in the load-control mode, and loading would cease when the axial displacement of a sample exceeded 3 mm. An initial force of 1 kN was applied prior to each test to ensure close contact between the sample and test machine head. The cyclic loading tests were loaded in two phases: a static loading phase and a cyclic loading-unloading phase, as shown in Figure 2. The loading rate was 0.2 kN/s in the static loading phase. In the cyclic loading-unloading phase, each sample was deformed over as many as 3000 cycles using a cosine waveform with a frequency of 0.5 Hz. Due to large time and computational costs, only a small number of cyclic loading tests could be performed with a relatively high frequency. The multilevel amplitude cyclic loading tests were carried out with specific experimental details described in Section 3.2.

3. Results and Discussion

3.1. Conventional Triaxial Compression Tests. Table 1 lists the test conditions and results for samples subjected to the conventional triaxial compression tests. The average axial, circumferential, and volumetric strain at the peak point were 0.011999530, −0.006169855, and −0.000340180, respectively. Figure 3 shows the entire deviatoric stress-strain curves. The limestone samples exhibited brittle behavior under a confining pressure of 10 MPa. In Figure 3, the symbols σ_1, σ_3, ε, ε_1, ε_3, and ε_v represent the axial stress, confining pressure, strain, axial strain, circumferential strain, and volumetric strain, respectively.

3.2. Cyclic Loading Tests. The experimental conditions and results for four samples subjected to the cyclic loading tests are listed in Table 2. The valley stress level is the ratio of corresponding valley stress to static strength, and the peak stress level is the ratio of corresponding peak stress to static strength. The average axial, circumferential, and volumetric strain at the failure point were 0.012433888, −0.007352870, and −0.002271853, respectively (Table 3). The absolute value of axial and circumferential strains at the failure point under cyclic loading was slightly larger than the corresponding values at the peak stress point in the conventional compression tests. This result is particularly important for evaluating the stability of rock mass subjected to cyclic loading. Point "a" in Figure 4 is defined as the failure point [3], and the maximum peak stress in each cycle cannot rise

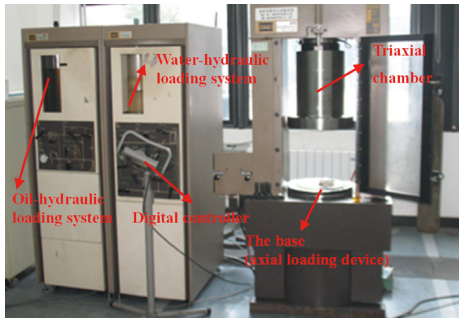

Figure 1: MTS815 rock mechanics test system.

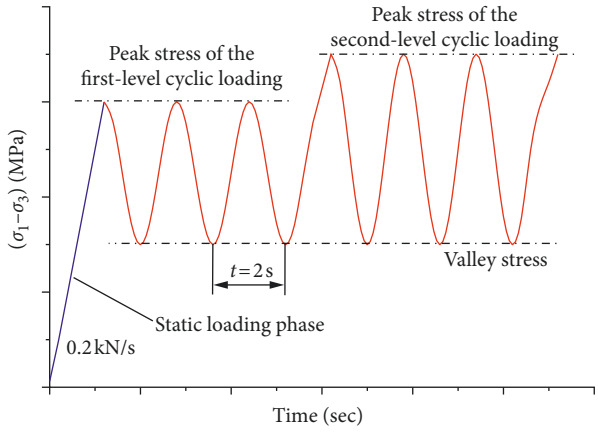

Figure 2: Diagram of the two loading phases in the cyclic loading tests.

above this point to the designed peak stress for a given cycle load.

The strength of different samples is known to vary. For example, sample SA. 6 has the lowest fatigue strength even though the deformation law applies equally to all samples subjected to cyclic loading. For analytical convenience, sample SA. 6 was chosen for further computational analysis. Figure 5 shows the deviatoric stress-strain curves of sample SA. 6.

3.2.1. Deformation. Figure 6 shows the maximum and minimum strain curves as a function of the loading cycle number (N) for sample SA. 6, excluding strain values after sample failure. One important observation is that the maximum or minimum strain values are not always obtained at the maximum or minimum stress points in a given cycle due to the rock's viscosity and plasticity during deformation.

In general, the remaining irreversible portion of strain after a given cycle is considered to be the residual strain [5]. Figure 7 shows the average residual strain induced by cyclic loading at different intervals and stress levels, excluding the very large residual strain amplitude at the 397th cycle. It should be further noted that the segment interval in Figure 7 is not evenly divided.

Residual axial, circumferential, and volumetric strains decreased with N when the stress level of the cyclic loading was 30%–85%. After 400 cycles, the strain values increase linearly, but little residual strain was produced each cycle. Under the test conditions of 3000 loading-unloading times in this stress level, the deformation of sample SA. 6 exhibited two phases: primary and steady.

Sample SA. 6 failed in the 397th loading cycle when the stress level of cyclic loading was 30%–87.5%. At this stress level, the sample's deformation exhibited three phases: primary, steady, and acceleration (Figure 7). In the primary phase (cycles 1–40), the residual strain triggered by cyclic loading decreased with N at a decreasing rate. In the steady phase (cycles 41–340), the residual strain remained mostly constant. In the acceleration phase (cycles 341–397), the residual strain increased with N at an increasing rate, which also indicated that the sample was close to failure.

The stress amplitude difference between the first- and second-level cyclic loadings with the same valley stress for sample SA. 6 was 2.5% (Figures 6 and 7). In the primary phase, the absolute amplitudes of the residual axial, circumferential, and volumetric strains induced by the second-level cyclic loading were lower than corresponding residual strains from the first-level cyclic loading. The former loading process had a strong influence on deformation in the primary phase under subsequent cyclic loading.

The properties of hysteresis loops in different phases of fatigue failure are distinctly different, as shown in Figure 8. Circumferential and volumetric deformations are more sensitive to fatigue failure than axial strain because both the amplitude values and change rates of the former are larger than those of axial strain when the sample is close to failure (Figure 7). The variation of hysteretic loops can therefore be used as an indicator to evaluate and predict fatigue failure.

3.2.2. Elastic Modulus. Figure 9 shows the elastic modulus evolution process of sample SA. 6 as a function of cycle number, excluding the unloading elastic modulus (−2800.24 MPa) of the last cycle at the 2nd cyclic loading. The unloading elastic modulus is larger than the loading elastic modulus except for the last cycle at the failure-amplitude loading (i.e., 2nd cyclic loading). Both elastic moduli increase with cycle number during the first several cycles in each amplitude level of cyclic loading, which indicates a decrease of residual axial strain. The two elastic moduli then decrease and fluctuate with cycle number. This observation implies that neither elastic moduli are suitable for describing the rock damage evolution process because damage increases and does not fluctuate with cycle number.

3.2.3. Energy Dissipation. Rock deformation and failure modes are closely related to energy dissipation. Trends in energy evolution in the rock deformation process can therefore reflect essential rock damage and failure characteristics. In the cyclic loading test, part of the energy absorbed by the rock is stored in the form of elastic strain energy; the remaining dissipation energy is consumed in the forms of heat and radiation [16]. In the triaxial test, the sample is subjected to both axial force and confining pressure exerted by the test machine. The energy for the

Table 1: Test results of the limestone samples in the conventional triaxial compression tests.

Sample number	Confining pressure (MPa)	Loading rate (mm/s)	Strains at the peak stress point			Peak strength (MPa)	Average strength (MPa)
			Axial	Circumferential	Volumetric		
SA. 10	10.0	0.003	0.012177853	−0.006236218	−0.000294582	78.29	
SA. 11	10.0	0.003	0.011894353	−0.006131956	−0.000369558	74.49	77.90
SA. 17	10.0	0.003	0.011926385	−0.006141393	−0.000356401	80.91	

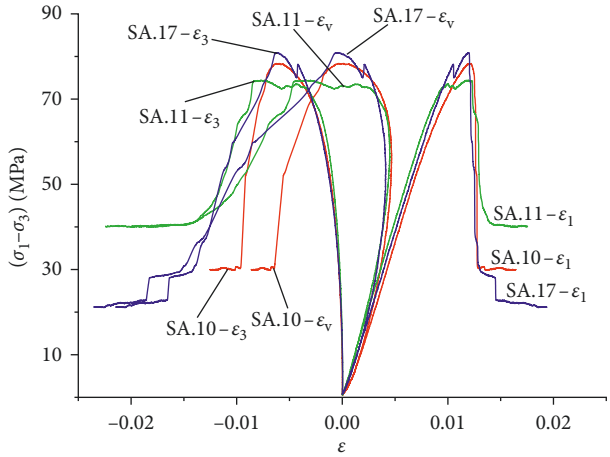

Figure 3: Deviatoric stress-strain curves from the triaxial compression tests of the limestone samples with a single loading rate (0.003 mm/s).

Table 2: Test conditions and results for the cyclic loading tests.

Sample number	Cyclic loading level	Valley stress level (%)	Peak stress level (%)	Amplitude level (%)	Cyclic number	Failure state
SA. 6	1	30	85	55	3000	Not failed
	2	30	87.5	57.5	397	Failed
SA. 7	1	30	85	55	3000	Not failed
	2	30	87.5	57.5	3000	Not failed
	3	30	90	60	3000	Not failed
	4	30	92.5	62.5	3000	Not failed
	5	30	95	65	3000	Not failed
	6	30	97.5	67.5	247	Failed
SA. 8	1	30	80	50	3000	Not failed
	2	30	85	55	3000	Not failed
	3	30	90	60	3000	Not failed
	4	30	92.5	62.5	2075	Failed
SA. 9	1	30	80	50	3000	Not failed
	2	30	85	55	3000	Not failed
	3	30	90	60	3000	Not failed
	4	30	92.5	62.5	3000	Not failed
	5	30	95	65	85	Failed

Table 3: Strain at the sample failure point in the cyclic loading tests.

Sample number	Strains at failure point		
	Axial	Circumferential	Volumetric
SA. 6	0.012548644	−0.007743632	−0.00293862
SA. 7	0.013142596	−0.006726573	−0.000310550
SA. 8	0.011629031	−0.007080188	−0.002531345
SA. 9	0.012415280	−0.007861088	−0.003306896

sample's axial deformation per unit volume is represented by U_1, the energy per unit volume by which the confining pressure suppresses the sample's circumferential deformation is given by U_3, and the dissipation energy per unit volume is given by U. These can, respectively, be expressed as

$$U_1 = \int \sigma_1 d\varepsilon_1,$$
$$U_3 = 2\int \sigma_3 d\varepsilon_3, \quad (1)$$
$$U = U_1 + U_3.$$

For triaxial cyclic loading tests, Zhang [23] showed that U_1 and U_3 are represented by the axial and circumferential hysteresis loop areas, respectively. In this paper, the

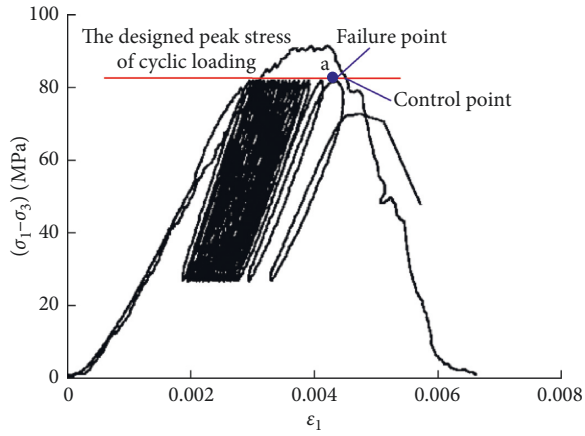

Figure 4: Diagram of the failure point and control point [22].

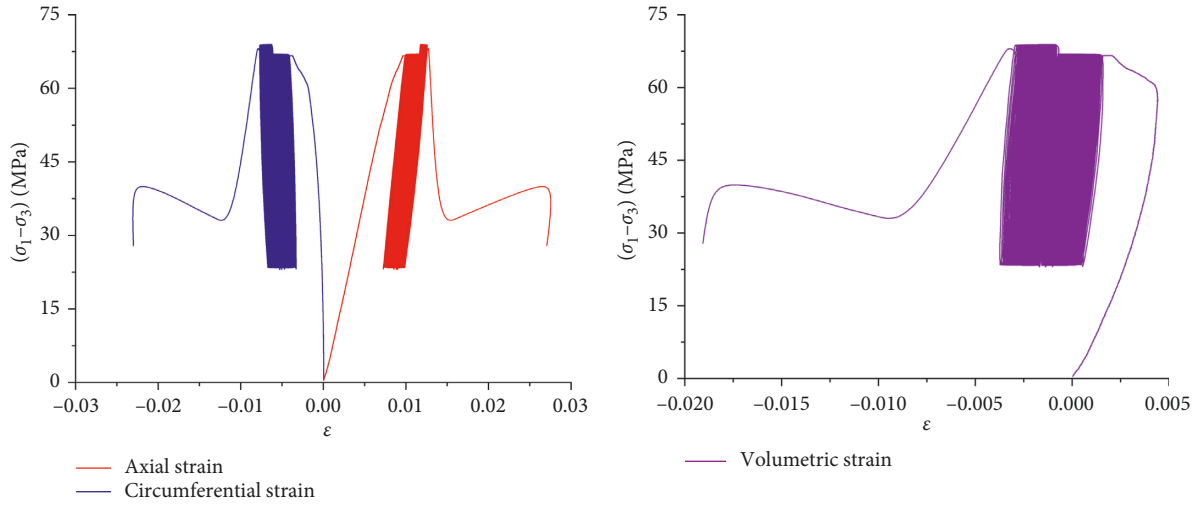

Figure 5: Deviatoric stress-strain curves of limestone sample SA. 6 in the cyclic loading test: (a) deviatoric stress-axial strain and deviatoric stress-circumferential strain curves and (b) deviatoric stress-volumetric strain curve.

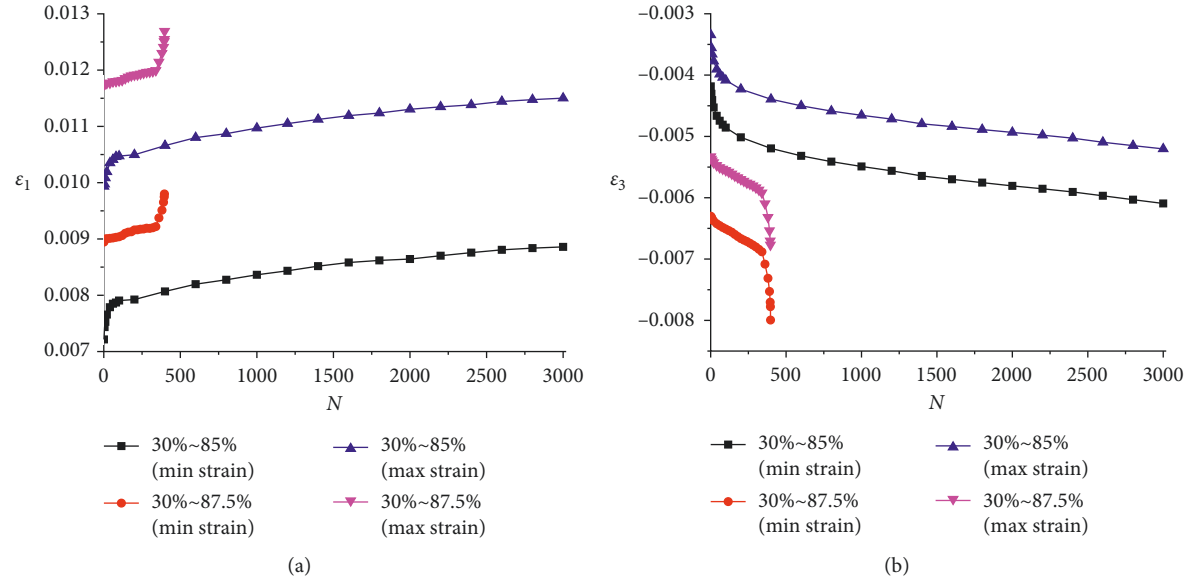

Figure 6: Continued.

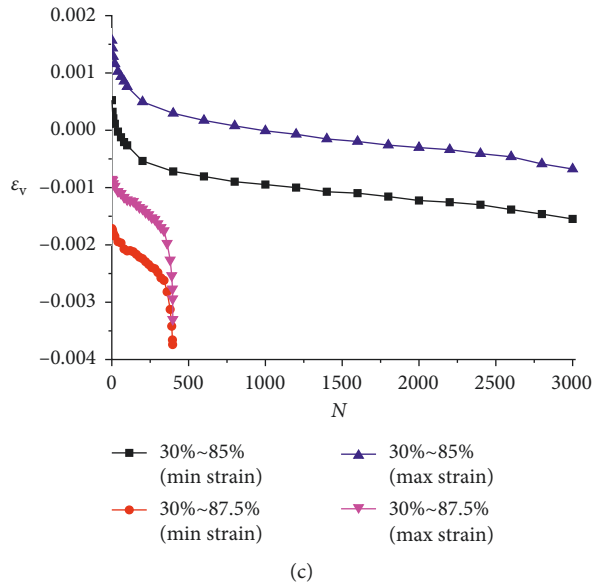

(c)

Figure 6: Maximum and minimum strain evolution for sample SA. 6 at different cyclic loading levels as a function of cycle number: (a) axial strain, (b) circumferential strain, and (c) volumetric strain.

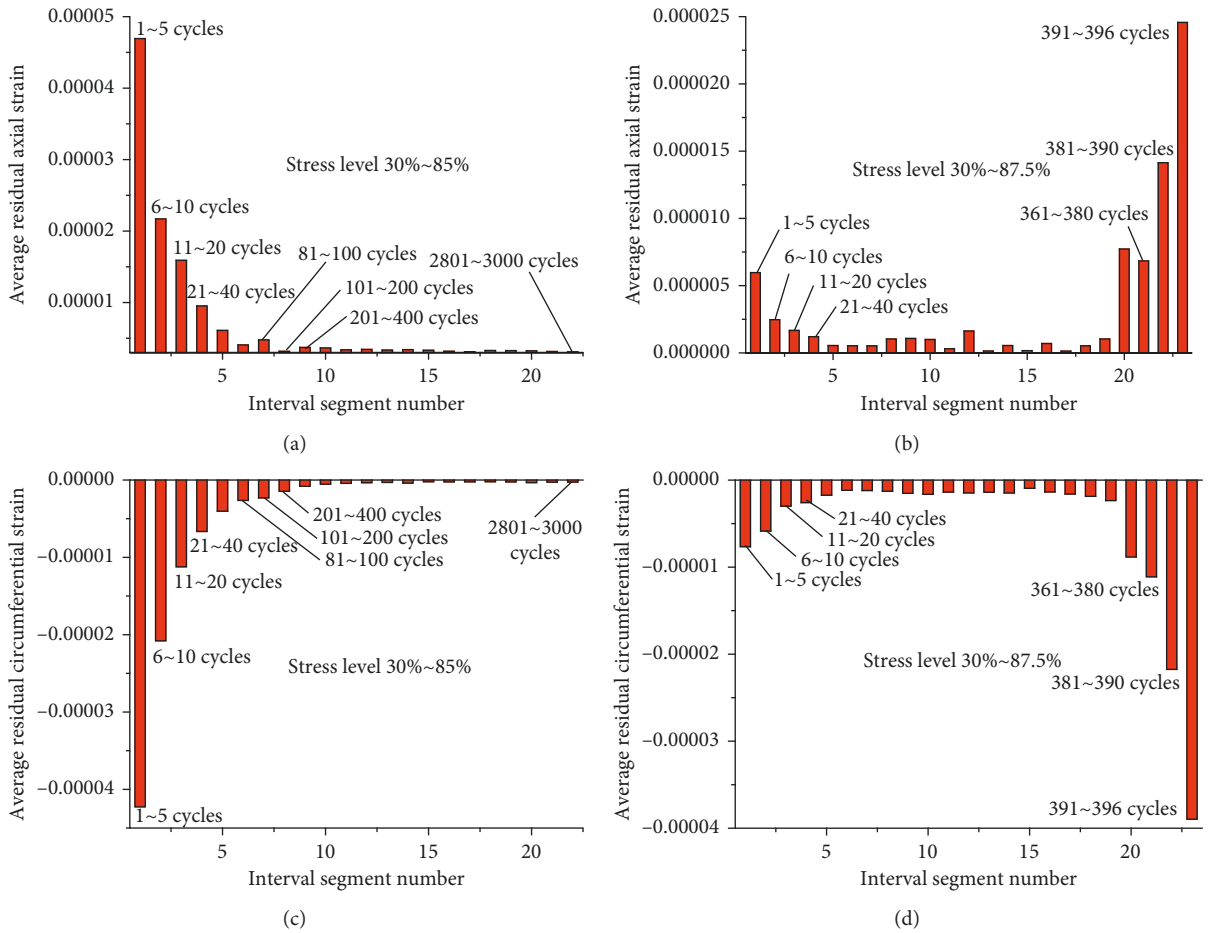

Figure 7: Continued.

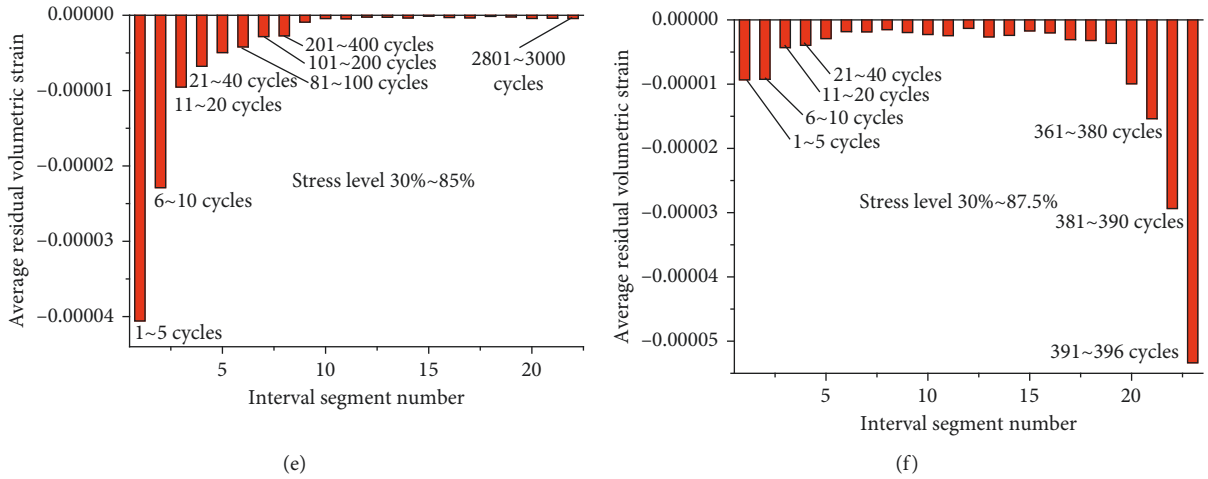

Figure 7: Average residual axial strain in different intervals at a stress level of (a) 30%–85% and (b) 30%–87.5%. Average residual circumferential strain in different intervals at a stress level of (c) 30%–85% and (d) 30%–87.5%. Average residual volumetric strain in different intervals at a stress level of (e) 30%–85% and (f) 30%–87.5%.

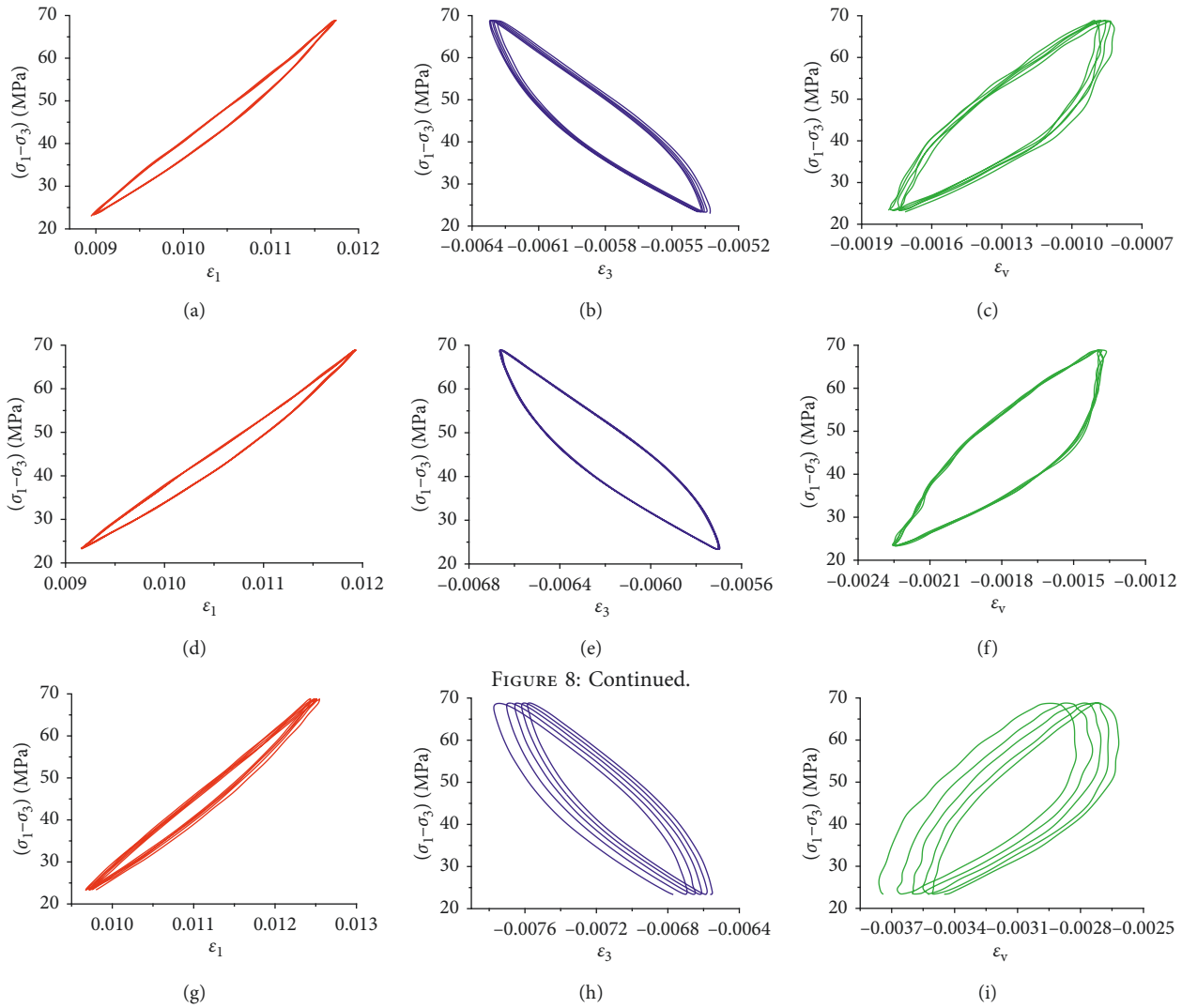

Figure 8: Continued.

Figure 8: Comparison of deviatoric stress-strain hysteresis loops of limestone sample SA. 6 in different phases of fatigue failure at the failure stress level: (a) axial, (b) circumferential, and (c) volumetric hysteresis loops for cycles 2 to 6; (d) axial, (e) circumferential, and (f) volumetric hysteresis loops for cycles 199 to 203; and (g) axial, (h) circumferential, and (i) volumetric hysteresis loops for the last five cycles before failure.

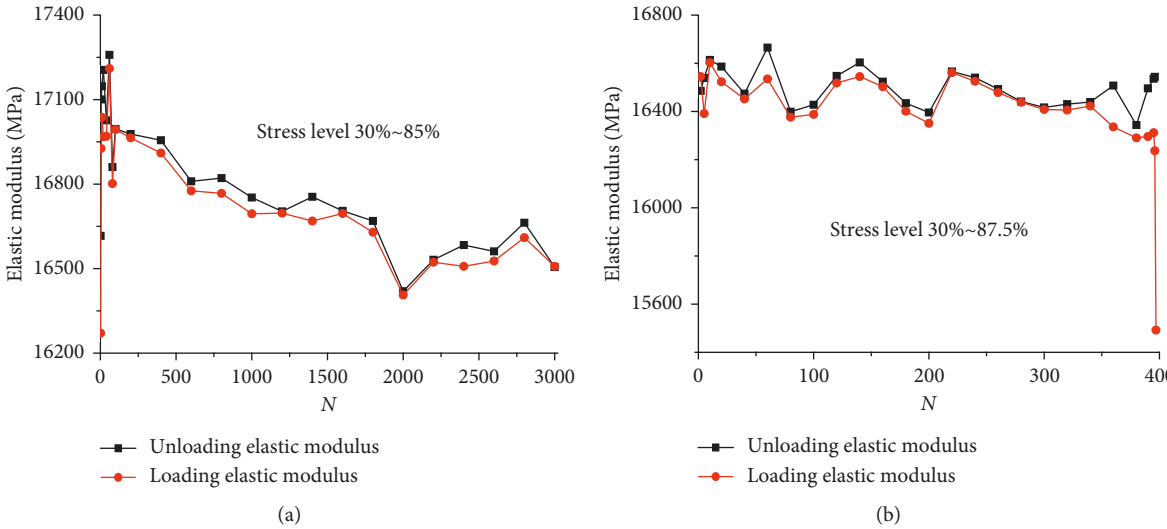

FIGURE 9: Elastic modulus versus cycle number curves of limestone sample SA. 6 at different amplitudes of cyclic loading during the (a) first stress level and (b) second stress level.

calculating method for hysteresis loop area is illustrated in the example shown in Figure 10.

In Figure 10(a), the area under the axial loading curve (area ABCD) is the axial unit volume energy for a loading-unloading cycle, expressed as U_{1+}. The area under the axial unloading curve (area A'B'CD) is the axial elastic strain energy per unit volume for a loading-unloading cycle, expressed as U_{1-}. Because U_+ is positive and U_- is negative, the sum of the two is the axial dissipated energy per unit volume, U_1, which can be obtained by integrating the trapezoidal areas shown in Figure 10(a). The energy calculation method using the confining pressure is the same as that by the axial pressure and can be analyzed according to Figure 10(b). The relationships between U_1/U_3, U_{1+}/U_{3+}, and U_{1-}/U_{3-} are

$$\begin{aligned} U_1 = U_{1+} + U_{1-} = \frac{1}{2}\Bigg(& \sum_{i=1}^{m}\left(\sigma_{1+,i} + \sigma_{1+,i+1}\right)\cdot\left(\varepsilon_{1+,i+1} - \varepsilon_{1+,i}\right) \\ & + \sum_{i=1}^{n}\left(\sigma_{1-,i} + \sigma_{1-,i+1}\right)\cdot\left(\varepsilon_{1-,i+1} - \varepsilon_{1-,i}\right)\Bigg), \\ U_3 = U_{3+} + U_{3-} = \Bigg(& \sum_{i=1}^{m}\left(\sigma_{3+,i} + \sigma_{3+,i+1}\right)\cdot\left(\varepsilon_{3+,i+1} - \varepsilon_{3+,i}\right) \\ & + \sum_{i=1}^{n}\left(\sigma_{3-,i} + \sigma_{3-,i+1}\right)\cdot\left(\varepsilon_{3-,i+1} - \varepsilon_{3-,i}\right)\Bigg), \end{aligned} \tag{2}$$

where U_{3+} represents the circumferential unit volume energy, U_{3-} is the circumferential elastic strain energy per unit volume, $\sigma_{1+,i}$ is the axial stress corresponding to the ith sampling point on the loading curve, $\varepsilon_{1+,i}$ is the axial strain corresponding to $\sigma_{1+,i}$, $\sigma_{1-,i}$ is the axial stress corresponding to the ith sampling point on the unloading curve, $\varepsilon_{1-,i}$ is the axial strain corresponding to $\sigma_{1-,i}$, $\sigma_{3+,i}$ is the confining pressure corresponding to the ith sampling point on the axial loading curve, $\varepsilon_{3+,i}$ is the circumferential strain corresponding to $\sigma_{3+,i}$, $\sigma_{3-,i}$ is the confining pressure corresponding to the ith sampling point on the axial unloading curve, and $\varepsilon_{3-,i}$ is the circumferential strain corresponding to $\sigma_{3-,i}$.

Figure 11 shows the relationships between dissipated energy and loading cycle number. In the first stress level, the dissipated energy per unit volume curve is L-shaped, indicating that the sample did not fail. In the second stress level, the dissipated energy per unit volume curve is U-shaped and can be divided into primary, steady, and acceleration phases. Figure 12 compares the three phases of strain and dissipated energy of sample SA. 6 in the second-level cyclic loading. From Figure 12, it can be seen that the three phases of dissipated energy evolution are consistent with those of the axial, circumferential, and volumetric deformations. Therefore, energy dissipation characteristics can also reflect a sample's fatigue damage evolution process.

4. Fatigue Damage Evolution

Damage is a process of nucleation, growth, and propagation of microcracks and microdefects that can degrade many material properties, including the elastic modulus, hardness, ultrasonic wave velocity, and residual strength. As such, all of the above parameters can be chosen as variables to describe the rock damage evolution process. Xiao et al. [21] proposed that a reasonable damage variable must meet the following basic requirements: (1) have a distinct physical meaning, (2) be easily measured and conveniently applied in engineering, (3) its evolution law should coincide well with the actual material degradation process, and (4) can account for zero-cycle damage. Based on these ideas, the elastic modulus method and residual strain method are clearly suitable to describe rock damage evolution.

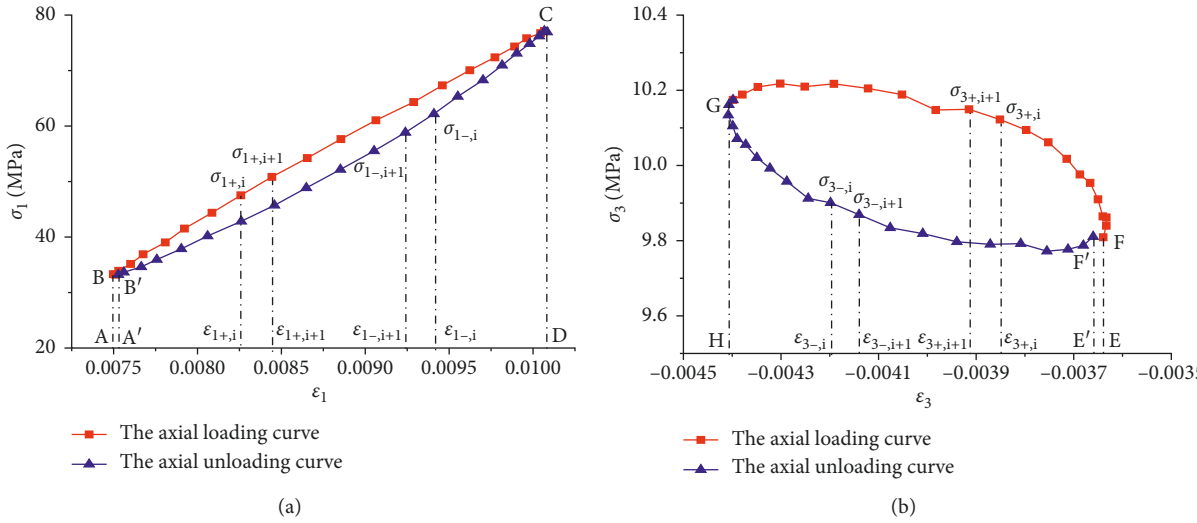

FIGURE 10: Method for calculating the hysteresis loop area (dissipated energy per unit volume): (a) σ_1-ε_1 hysteresis loop area (U_1) and (b) σ_3-ε_3 hysteresis loop area (U_3).

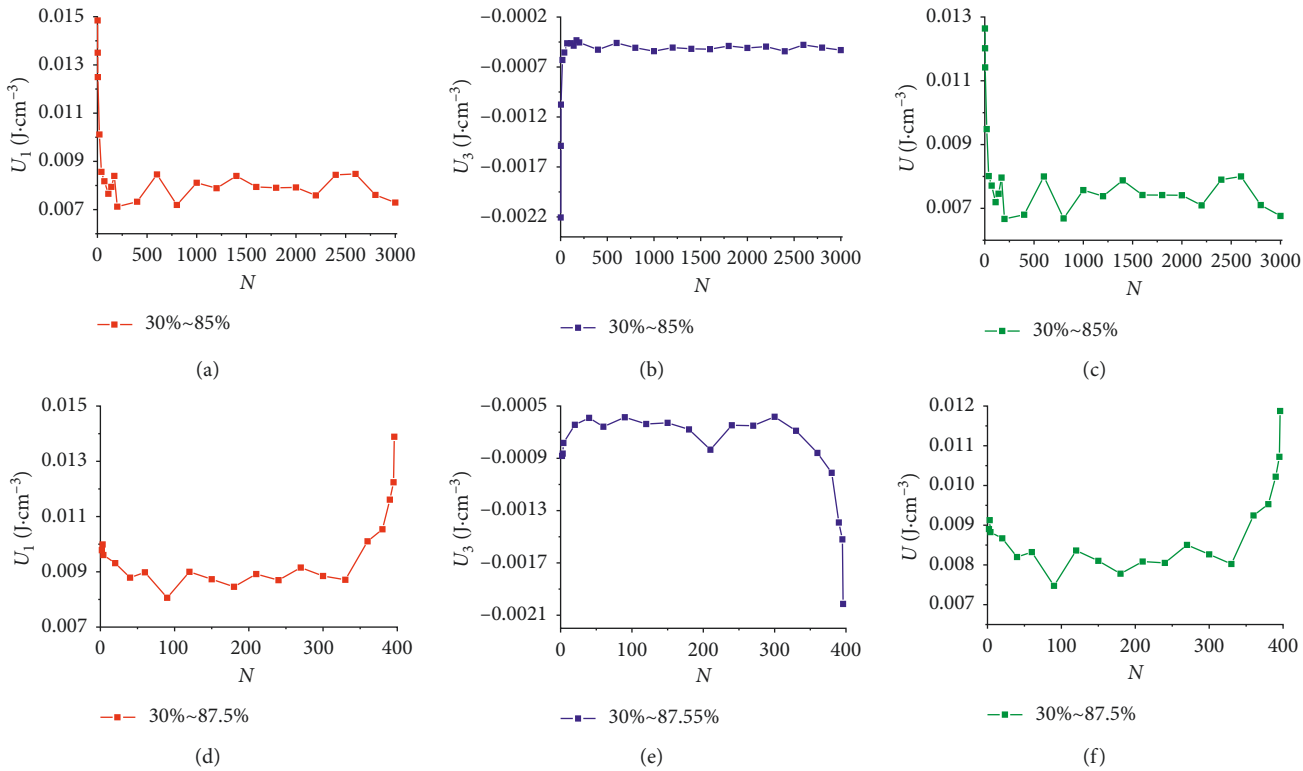

FIGURE 11: Dissipated energy versus loading cycle number curves at varying stress levels for limestone sample SA. 6: (a) axial, (b) circumferential, and (c) total dissipated energies per unit volume at the first stress level and (d) axial, (e) circumferential, and (f) total dissipated energies per unit volume at the second stress level.

The damage variable in the classical elastic modulus method is defined as [17]

$$D = 1 - \frac{E'}{E}, \tag{3}$$

where E' is Young's modulus of the damaged material and E is the initial elastic modulus. Xie et al. [17] argued that (3) can only be applied for the calculation of elastic damage and proposed a new damage definition for elastic-plastic materials:

$$D = 1 - \frac{\varepsilon - \varepsilon'}{\varepsilon} \frac{E_d}{E}, \tag{4}$$

where Ed is the unloading elastic modulus of the elastic-plastic material and ε' is the residual plastic deformation

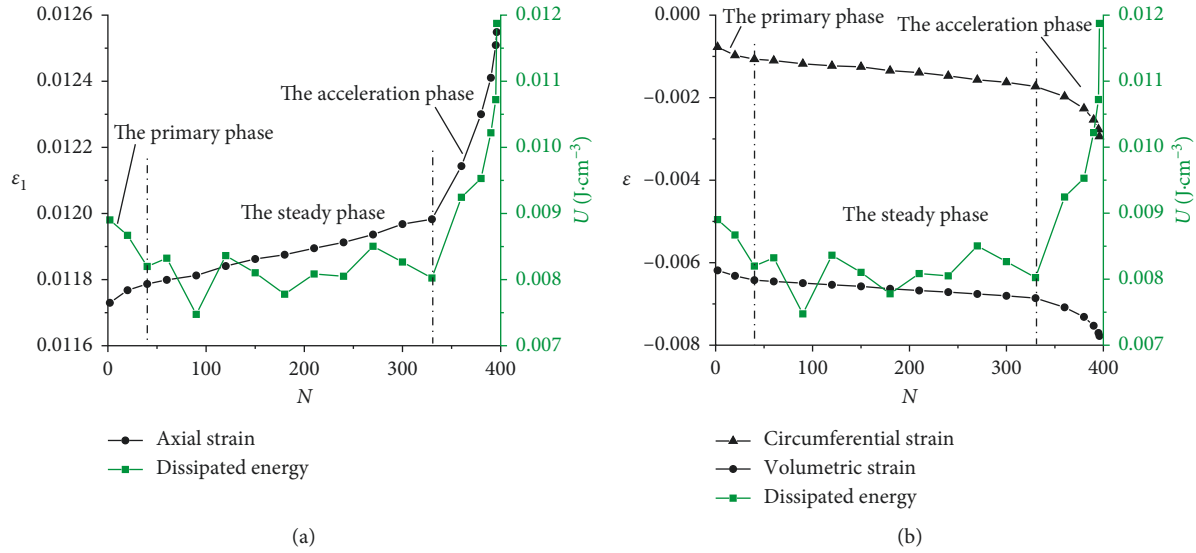

FIGURE 12: Comparison of the three phases of strain and dissipated energy evolution: (a) axial strain and dissipated energy and (b) circumferential strain, volumetric strain, and dissipated energy.

after unloading in a given cycle. However, the unloading elastic modulus is sometimes larger than the initial elastic modulus, but only when the damage increases to a certain extent and the unloading elastic modulus begins to decrease with N [24]. In most cases, the amplitude of the unloading elastic modulus changes and fluctuates with increasing cycle number (Figure 9). As a consequence, this method can only be used to describe the rock damage evolution process under certain circumstances.

Deformation is the most direct manifestation form of rock failure and occurs continuously before failure. As such, the damage variable defined by the strain method can well describe the rock's damage evolution process. Li et al. [18] defined the damage variable as

$$D = \frac{\varepsilon - \varepsilon_0}{\varepsilon_d - \varepsilon_0} \frac{\varepsilon_d}{\varepsilon}, \tag{5}$$

where ε0 is the axial strain at the beginning of cyclic loading when damage D = 0, εd is the axial strain at the end of cyclic loading when $D = 1$, and ε is the axial strain at the end of a given loading cycle. Zero-cycle damage (i.e., damage caused by monotonic loading before the application of cyclic loading) is ignored in (5).

Xiao et al. [21] defined the damage variable as

$$D = \frac{\varepsilon_r^n}{\varepsilon_r^f}, \tag{6}$$

where ε_r^n and ε_r^f are the residual strain after the nth cycle and the ultimate residual strain to fatigue failure, respectively. The zero-cycle damage in (6) is actually larger than the true zero-cycle damage because residual strain in the initial compaction phase is used for the damage calculation. However, it is widely accepted that damage does not occur during the compaction phase [25].

We have therefore established a formula that considers zero-cycle damage:

$$D = \frac{\varepsilon - \varepsilon_0 + \varepsilon_{p0}}{\varepsilon_d - \varepsilon_0 + \varepsilon_{p0}}, \tag{7}$$

where ε_{p0} is the plastic strain that causes zero-cycle damage, excluding plastic strain in the compaction phase. The calculation method is shown in Figure 13. The accumulation of residual axial strain indicates increasing damage. D has a value of zero prior to the elastic phase and is equal to 1 at failure. Because a certain residual strain is produced in each loading-unloading cycle, (7) can better reflect the zero cycle of rock damage.

Figure 14 shows the relationship between the damage variable and loading cycle number for sample SA. 6. The zero-cycle damage D_0 was 0.2842. The damage values at the end of the first- and second-level cyclic loading processes were 0.7396 and 0.7632, respectively, and 1.0 upon failure. In this test, the damage induced by cyclic loading-unloading accounted for 69.22% of the total damage and the rest was caused by static loading.

5. Conclusions

The fatigue properties of limestone samples subjected to multilevel amplitude cyclic loadings were investigated using an MTS815.02 rock mechanics test system. Based on the test results, the following conclusions can be drawn:

(1) The absolute amplitudes of axial and circumferential strains at the failure point induced by cyclic loading were slightly larger than those of the corresponding strains at the peak stress point by conventional compression tests. This result is important for evaluating the stability of rock mass.

(2) The first-level cyclic loading process has a strong influence on rock deformation in the primary phase under the second-level of cyclic loading. A smaller difference in stress amplitude between the two cyclic

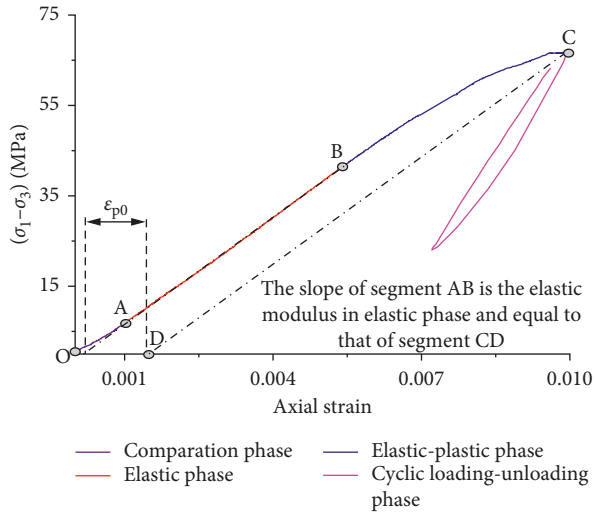

Figure 13: Calculation of the parameter ε_{p0}.

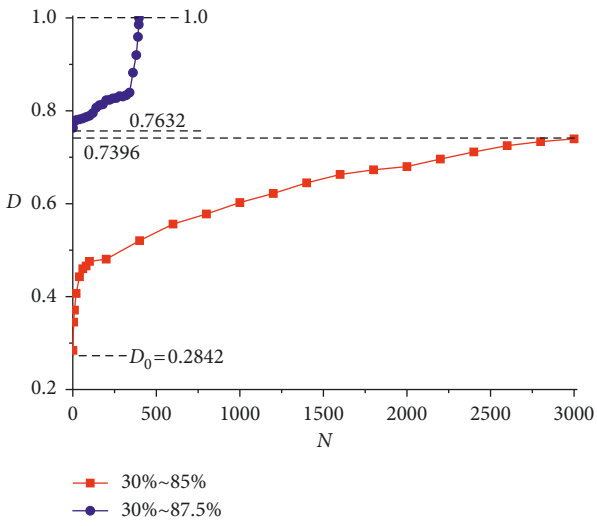

Figure 14: Relationship between the damage variable and loading cycle number for sample SA. 6.

loading levels leads to less rock deformation triggered by the latter.

(3) Circumferential and volumetric deformations are more sensitive to failure fatigue than axial deformation, and the variation of hysteretic loops can reflect a rock's damage evolution process.

(4) The three phases of dissipated energy evolution are consistent with those of the sample's deformation such that energy dissipation characteristics can reflect a sample's fatigue damage evolution process.

(5) A concise damage formula is proposed that can better describe zero-cycle damage and the damage evolution process.

Data Availability

The data used to support the findings of this study are available from the corresponding author upon request.

Conflicts of Interest

The authors declare that they have no conflicts of interest.

Acknowledgments

This research was supported by the National Natural Science Foundation of China (Grant nos. 51379116 and 51574156), Tai'shan Scholar Talent Team Support Plan for Advantaged and Unique Discipline Areas, and Program for Graduate Science and Technology Innovation of Shandong University of Science and Technology in 2017 (nos. SDKDYC170204 and SDKDYC170214). We thank Kathy Sole, Ph.D., and Esther Posner, Ph.D., from Liwen Bianji, Edanz Group China (www.liwenbianji.cn/ac), for editing the English text of a draft of this manuscript.

References

[1] P. Wang, L. S. Jiang, J. Q. Jiang, P. Q. Zheng, and W. Li, "Strata behaviors and rock burst-inducing mechanism under the coupling effect of a hard, thick stratum and a normal fault," *International Journal of Geomechanics*, vol. 18, no. 2, Article ID 04017135, 2018.

[2] Z. C. Wang, S. C. Li, L. P. Qiao, and J. G. Zhao, "Fatigue behavior of granite subjected to cyclic loading under triaxial compression condition," *Rock Mechanics and Rock Engineering*, vol. 46, no. 6, pp. 1603–1615, 2013.

[3] X. R. Ge, Y. Jiang, Y. D. Lu, and J. X. Ren, "Testing study on fatigue deformation law of rock under cyclic loading," *Chinese Journal of Rock Mechanics and Engineering*, vol. 22, no. 10, pp. 1581–1585, 2003.

[4] Q. X. Zhang, X. R. Ge, M. Huang, and H. Sun, "Testing study on fatigue deformation law of red-sandstone under triaxial compression with cyclic loading," *Chinese Journal of Rock Mechanics and Engineering*, vol. 25, no. 3, pp. 473–478, 2006.

[5] G. M. Lu, Y. H. Li, X. W. Zhang, and J. P. Liu, "Fatigue deformation characteristics of yellow sandstone under cyclic loading," *Chinese Journal of Geotechnical Engineering*, vol. 37, no. 10, pp. 1886–1892, 2015.

[6] E. L. Liu and S. M. He, "Effects of cyclic dynamic loading on the mechanical properties of intact rock samples under confining pressure conditions," *Engineering Geology*, vol. 125, pp. 81–91, 2012.

[7] A. Momeni, M. Karakus, G. R. Khanlari, and M. Heidari, "Effects of cyclic loading on the mechanical properties of a granite," *International Journal of Rock Mechanics and Mining Sciences*, vol. 77, pp. 89–96, 2015.

[8] G. M. Lu and Y. H. Li, "Influence of confining pressure on fatigue deformation properties of yellow sandstone," *Rock and Soil Mechanics*, vol. 37, no. 7, pp. 1847–1856, 2016.

[9] C. L. Feng, X. Q. Wu, D. X. Ding, and Y. F. Wu, "Investigation on fatigue characteristics of white sandstone under cyclic loading," *Chinese Journal of Rock Mechanics and Engineering*, vol. 28, no. S1, pp. 2749–2754, 2009.

[10] C. H. Shi, Z. D. Ding, M. F. Lei, and L. M. Peng, "Accumulated deformation behavior and computational model of water-rich mudstone under cyclic loading," *Rock Mechanics and Rock Engineering*, vol. 47, no. 4, pp. 1485–1491, 2014.

[11] M. N. Bagde and V. Petroš, "Fatigue properties of intact sandstone samples subjected to dynamic uniaxial cyclical loading," *International Journal of Rock Mechanics and Mining Sciences*, vol. 42, no. 2, pp. 237–250, 2005.

[12] K. Fuenkajorn and D. Phueakphum, "Effects of cyclic loading on mechanical properties of Maha Sarakham salt," *Engineering Geology*, vol. 112, no. 1–4, pp. 43–52, 2010.

[13] W. G. Liang, Y. S. Zhao, S. G. Xu, and M. B. Dusseault, "Effects of strain rate on the mechanical properties of salt rock," *International Journal of Rock Mechanics and Mining Sciences*, vol. 48, no. 1, pp. 161–167, 2011.

[14] D. Y. Jiang, J. Y. Fan, J. Chen, L. Li, and Y. Cui, "A mechanism of fatigue in salt under discontinuous cycle loading," *International Journal of Rock Mechanics and Mining Sciences*, vol. 86, pp. 255–260, 2016.

[15] J. Y. Fan, J. Chen, D. Y. Jiang, A. Chemenda, J. C. Chen, and J. Ambre, "Discontinuous cyclic loading tests of salt with acoustic emission monitoring," *International Journal of Fatigue*, vol. 94, no. 1, pp. 140–144, 2017.

[16] M. M. He, Y. S. Chen, N. Li, and C. H. Zhu, "Deformation and energy characteristics of sandstone subjected to uniaxial cyclic loading," *Journal of China Coal Society*, vol. 40, no. 8, pp. 93–99, 2015.

[17] H. P. Xie, Y. Ju, and L. Dong, "Discussion about "elastic modulus method" in the classic definition of damage," *Mechanics and Practice*, vol. 19, no. 2, pp. 1–5, 1997.

[18] S. C. Li, J. Xu, Y. Q. Tao, X. J. Tang, and H. W. Yang, "Low cycle fatigue damage model and damage variable expression of rock," *Rock and Soil Mechanics*, vol. 30, no. 6, pp. 1611–1615, 2009.

[19] J. Q. Xiao, D. X. Ding, F. L. Jiang, and X. Gen, "Parameters estimation method of fatigue damage model of rock," *Rock and Soil Mechanics*, vol. 30, no. 6, pp. 1635–1638, 2009.

[20] J. Q. Xiao, *Theoretical and experimental investigation on fatigue properties of rock under cyclic loading*, Ph.D. thesis, Central South University, Changsha, Hu'nan, China, 2009.

[21] J. Q. Xiao, D. X. Ding, F. L. Jiang, and X. Gen, "Fatigue damage variable and evolution of rock subjected to cyclic loading," *International Journal of Rock Mechanics and Mining Sciences*, vol. 47, no. 3, pp. 461–468, 2010.

[22] X. R. Ge, "Deformation control law of rock fatigue failure, real-time X-ray CT scan of geotechnical testing, and new method of stability analysis of slopes and dam foundations," *Chinese Journal of Geotechnical Engineering*, vol. 30, no. 1, pp. 1–20, 2008.

[23] Y. Zhang, "*Experimental research on characteristics of deformation and dissipated energy of rock under cyclic loading conditions*," M.S. thesis, Chongqing University, Chongqing, China, 2011.

[24] B. Sun, Z. D. Zhu, C. Shi, and Z. H. Luo, "Dynamic mechanical behavior and fatigue damage evolution of sandstone under cyclic loading," *International Journal of Rock Mechanics and Mining Sciences*, vol. 94, pp. 82–89, 2017.

[25] Y. Y. Li, *Deformation and failure characteristics and energy evolution laws of coal-rock mass under mining influence*, Ph.D. thesis, Shandong University of Science and Technology, Qingdao, Shandong, China, 2015.